Direct assignment of EPR spectra to structurally defined iron-sulfur clusters in complex I by double electron–electron resonance

Maxie M. Roessler[a,b], Martin S. King[c], Alan J. Robinson[c], Fraser A. Armstrong[b], Jeffrey Harmer[a,1], and Judy Hirst[c,1]

[a]Center for Advanced Electron Spin Resonance, and [b]Inorganic Chemistry Laboratory, Department of Chemistry, University of Oxford, South Parks Road, Oxford, OX1 3QR, United Kingdom; and [c]Medical Research Council Mitochondrial Biology Unit, Wellcome Trust/Medical Research Council Building, Hills Road, Cambridge, CB2 0XY, United Kingdom

Edited by David Britt, University of California, Davis, Davis, CA, and accepted by the Editorial Board November 25, 2009 (received for review July 20, 2009)

In oxidative phosphorylation, complex I (NADH:quinone oxidoreductase) couples electron transfer to proton translocation across an energy-transducing membrane. Complex I contains a flavin mononucleotide to oxidize NADH, and an unusually long series of iron-sulfur (FeS) clusters, in several subunits, to transfer the electrons to quinone. Understanding coupled electron transfer in complex I requires a detailed knowledge of the properties of individual clusters and of the cluster ensemble, and so it requires the correlation of spectroscopic and structural data: This has proved a challenging task. EPR studies on complex I from *Bos taurus* have established that EPR signals N1b, N2 and N3 arise, respectively, from the 2Fe cluster in the 75 kDa subunit, and from 4Fe clusters in the PSST and 51 kDa subunits (positions 2, 7, and 1 along the seven-cluster chain extending from the flavin). The other clusters have either evaded detection or definitive signal assignments have not been established. Here, we combine double electron-electron resonance (DEER) spectroscopy on *B. taurus* complex I with the structure of the hydrophilic domain of *Thermus thermophilus* complex I. By considering the magnetic moments of the clusters and the orientation selectivity of the DEER experiment explicitly, signal N4 is assigned to the first 4Fe cluster in the TYKY subunit (position 5), and N5 to the all-cysteine ligated 4Fe cluster in the 75 kDa subunit (position 3). The implications of our assignment for the mechanisms of electron transfer and energy transduction by complex I are discussed.

DEER | distance measurement | mitochondria | NADH:quinone oxidoreductase | pulsed EPR

Complex I (NADH:quinone oxidoreductase) is an essential respiratory enzyme. It is an entry point to the electron-transport chains of many aerobic organisms, and its dysfunction is linked to numerous human diseases by mitochondrial DNA mutations, decreased respiratory capacity and increased oxidative stress (1). Complex I is a complicated, membrane-bound enzyme that couples NADH oxidation and quinone reduction to proton translocation across an energy-transducing membrane. It comprises a membrane extrinsic (hydrophilic) domain, and a membrane intrinsic (hydrophobic) domain. A chain of iron-sulfur (FeS) clusters in the hydrophilic domain is essential in transferring electrons from the flavin mononucleotide at the site of NADH oxidation to the hydrophobic site of quinone reduction. The mechanism by which electron transfer drives proton translocation is not known. The 3.3 Å structure of the hydrophilic domain of *Thermus thermophilus* complex I, the only high resolution structure available, reveals how the FeS clusters and the flavin are arranged (2). Seven clusters form an extensive chain from the flavin to the quinone binding site; the eighth cluster, of unknown function, is on the opposite side of the flavin (see Fig. 1). A ninth cluster, more than 20 Å from the cluster chain, occurs in only a few species, including *T. thermophilus* and *Escherichia coli*. Current knowledge of the properties of the clusters, most obviously their reduction potentials, has been derived almost exclusively from X-band continuous wave (CW) EPR spectroscopy on complex I from *B. taurus* (bovine) heart mitochondria (3–6), which is closely related to human complex I.

To understand the mechanism of energy transduction by complex I, it is essential to assign the set of spectroscopically determined cluster properties to the set of structurally defined clusters. The correct assignment will define the properties of individual clusters (reduction potentials) and of the cluster ensemble (a basis for the free-energy profile for electron transfer along the chain) as required to interpret intramolecular electron transfer rates and identify possible energy coupling sites (8). However, not all of the FeS clusters have been detected by EPR, and the assignments of the observed EPR signals to the structurally defined clusters remain controversial (3–6). Five reduced FeS clusters are typically observed in complex I from *B. taurus* reduced by NADH, and their CW EPR spectra are denoted N1b, N2, N3, N4 and N5. Signal N1a, from 2Fe[24] (see Fig. 1 for our nomenclature), is exhibited by the 24 kDa subunit and the 24 + 51 kDa subcomplex, but not by complex I (6), so it is not relevant here. Fig. 1 presents the three contending assignments of signals to clusters. Signal N1b is from a 2Fe cluster, but not from 2Fe[24], so it is from 2Fe[75] (position 2 in the seven-cluster chain from 4Fe[51] to 4Fe[PS], see Fig. 1). Signals N3 and N2 are from 4Fe[51] (position 1) and 4Fe[PS] (position 7), respectively, because interactions with the flavosemiquinone (9) and ubisemiquinones (10) have been observed. Ohnishi's model (A) assigns N4 and N5 to 4Fe[75]C and 4Fe[75]H (positions 3 and 4), respectively (3, 4), whereas Hirst's models (B and C) assign N4 to one (or both) of 4Fe[TY]1 and 4Fe[TY]2 (positions 5 and 6), and N5 to 4Fe[75]C (position 3) (5, 6). Importantly, the assignments of N4 and N5 rely on data from overexpressed subunits, enzyme fragments, and point mutations, and thus on circumstantial evidence rather than on direct measurements on intact *B. taurus* complex I.

Here, we assign N4 directly by DEER spectroscopy (11). DEER uses the electron-electron dipolar interaction between two paramagnetic centers to ascertain their separation and relative orientation; it is well established for determining the distances between organic radicals (such as $NO^{\bullet}$) with $S = 1/2$ ground states and precisely known magnetic moments (12, 13). In contrast, applying DEER to metal sites in multicentered enzymes is a relatively new application that builds on the seminal

Author contributions: F.A.A., J. Harmer, and J. Hirst designed research; M.M.R., M.S.K., and A.J.R. performed research; M.M.R., J. Harmer, and J. Hirst analyzed data; M.M.R., M.S.K., A.J.R., F.A.A., J. Harmer, and J. Hirst wrote the paper.

The authors declare no conflict of interest.

This article is a PNAS Direct Submission. D.B. is a guest editor invited by the Editorial Board.

Freely available online through the PNAS open access option.

[1]To whom correspondence may be addressed. E-mail:jeffrey.harmer@chem.ox.ac.uk or jh@mrc-mbu.cam.ac.uk.

This article contains supporting information online at www.pnas.org/cgi/content/full/0908050107/DCSupplemental.

Downloaded by guest on October 25, 2021

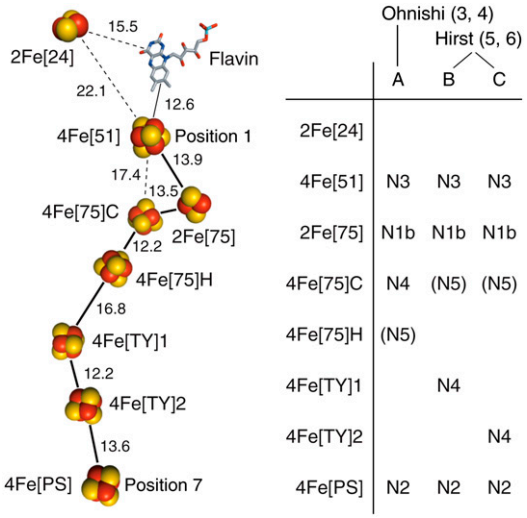

Fig. 1. Arrangement of the redox cofactors in *B. taurus* complex I, based on the structure from *T. thermophilus*, and possible assignments of EPR signals to clusters. *Left*: FeS clusters in the structure of the hydrophilic arm of *T. thermophilus* complex I [2FUG.PDB (2)] conserved in *B. taurus*, named according to their type (2Fe or 4Fe), subunit [according to the standard nomenclature for *B. taurus*, 75 = 75 kDa subunit, 51 = 51 kDa subunit, 24 = 24 kDa subunit, PS = PSST subunit, TY = TYKY subunit (7)], and differentiated when necessary by C (all cys ligated) or H (one his ligand), or as cluster 1 or 2. Distances are center-to-center for the FeS clusters or the central ring of the isoalloxazine system. (*Right*): Extant assignments of the five EPR signals observed in *B. taurus* complex I reduced by NADH (3–6). N5 is not addressed here.

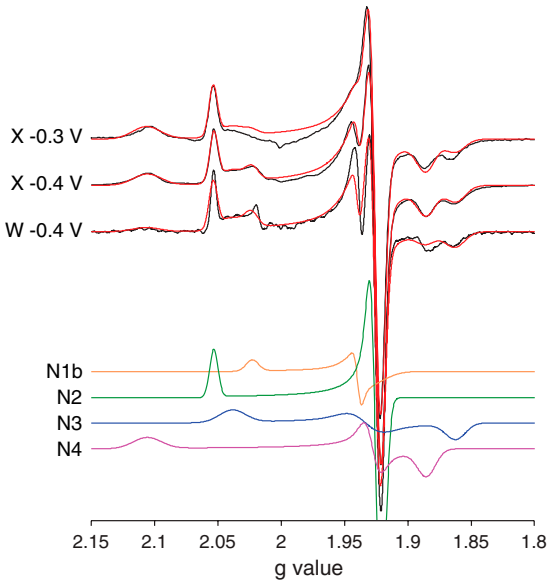

Fig. 2. EPR spectra of complex I from *B. taurus*, and simulations for N1b, N2, N3, and N4. X-band CW EPR spectra of complex I reduced to −0.4 V and −0.3 V were recorded at 12 K, at 9.408 and 9.393 GHz, respectively. The W-band (93.875 GHz) echo-detected EPR spectrum (numerical 1st derivative representation) of complex I reduced to −0.4 V was recorded at 8.5 K. The three spectra (*Black*) are compared to one another and to their simulated spectra (18) (*Red*, comprising N1b, N2, N3, and N4, see Table 1), by using the *g*-value scale. N1b, N2, N3, and N4 are shown for the −0.4 V X-band spectrum. At −0.3 V, N1b is essentially absent. See *Experimental Methods* section for the measurement parameters.

work of Bertrand (14) and Noodleman et al. (15) on FeS clusters, and on the application of DEER to a [NiFe]-hydrogenase by Bittl and coworkers (16, 17). First, the magnetic moment of a cluster results from ferromagnetic and antiferromagnetic coupling between the Fe subsites and varies with the cluster type and environment (14). Second, FeS EPR spectra are much broader than the microwave (mw) pulse excitation profiles of the DEER sequence, so each pulse selects only a limited range of molecular orientations. Therefore, a series of experiments, in which both the magnetic field and pulse frequencies are varied, must be combined. Here, we use the cluster positions defined by the structure of the hydrophilic domain of *T. thermophilus* complex I to simulate DEER traces for each of the models A, B and C, and compare them to our experimental data. Once N4 is assigned, the origin of N5 is deduced. Our assignment of N4 has direct implications for thermodynamic and kinetic models of electron transfer in complex I, and for future investigations of the mechanism of energy transduction.

Results

Determination of Principal *g* values and Linewidths for Signals N1b, N2, N3, and N4. EPR spectra of complex I from *B. taurus* recorded at X- and W-band are shown in Fig. 2. The spectra comprise four overlapping signals (N1b, N2, N3, and N4) from four reduced FeS clusters. Each signal is described by three principal *g* values and three *g*-strain parameters to describe the linewidths (see Table 1). As expected from their reduction potentials (3), N2, N3, and N4 contribute significantly at both −0.4 and −0.3 V (see Table 1). Signal N1b is substoichiometric (it is small at −0.4 V and essentially absent at −0.3 V) hence the cluster responsible has a more negative potential (6). Signal N5 is not observed because it is too fast-relaxing (it can only be observed clearly at lower temperatures, below 7 K (3, 6)). Importantly, the X- and W-band spectra essentially overlay when plotted on a *g*-value axis to remove the mw frequency/magnetic field dependence (see Fig. 2), indicating that the spectral peak positions correspond to the principal *g* values. Furthermore, any dipolar or exchange interactions between the EPR visible clusters must be less than ∼50 MHz, the X-band linewidth, indicating an intercluster distance greater than ∼10 Å (depending on the magnetic moments, see below).

DEER Traces from *B. taurus* Complex I. DEER spectroscopy employs two mw frequencies to isolate the dipolar interactions (see Fig. 3). The pulse sequence at frequency ω_A produces a refocused echo from the detection (A) spins; the pulse at frequency ω_B inverts the pump (B) spins, and changes the local field at the detection spins. The resulting DEER traces (see Figs. 4 and 5) show how the refocused echo intensity (modulated by the dipolar coupling frequencies) depends upon the timing of the pump pulse, t, within the detection pulse sequence. Different frequency combinations for ω_A and ω_B select different sets of orientations of a cluster pair with respect to the spectrometer's magnetic field, $\mathbf{B}_0$ (see Fig. 6 and Fig. S1), and each DEER trace comprises a set of dipolar frequencies, ω_{dd}, from the contributing cluster pair orientations:

$$\omega_{dd}^{m} = \frac{\mu_0 \beta^2}{2h} g_A^m g_B^m \sum_i \sum_j k_{Ai} k_{Bj} \frac{3\cos^2 \psi_{ij}^m - 1}{r_{ij}^3} \qquad [1]$$

The superscript m denotes a single orientation of the unit magnetic field vector $\mathbf{B}_0^m(\theta, \phi)$ with respect to the molecular frame (see Fig. 6 for the polar angles θ and ϕ); g values g_A and g_B are from cluster A (detection) and B (pump), respectively; ψ_{ij}^m defines the angle between $\mathbf{B}_0^m(\theta, \phi)$ and the Fe_{Ai}-Fe_{Bj} unit vector $\mathbf{n}_{ij}$; r_{ij} is the distance between i and j; and, k_{Ai} and k_{Bj} are the spin projection factors (SPFs) of each Fe (i of cluster A, j of cluster B). SPFs describe how the spins of the Fe subsites in a cluster couple magnetically to produce the observed $S = 1/2$ spin state. Then, the simulated DEER oscillation from a pair of clusters is:

$$y(t)_{sim} = \sum_m f_A^m (1 - c_{mod}^m (1 - \cos(\omega_{dd}^m t))). \qquad [2]$$

Downloaded by guest on October 25, 2021

Table 1. Principal *g* values, *g*-strain parameters, and relative intensities of spectra from the four reduced FeS clusters observed in *B. taurus* complex I

Signal	Principal *g* value*			*g* strain*			Amplitude (%)†	
	g_x	g_y	g_z	g_x	g_y	g_z	EPR	DEER
N1b	1.927	1.939	2.023	0.029	0.005	0.011	9 (3)	4 (1)
N2	1.921	1.927	2.054	0.009	0.008	0.008	32 (34)	61 (55)
N3	1.863	1.934	2.039	0.018	0.027	0.024	26 (23)	9 (13)
N4	1.886	1.928	2.107	0.017	0.012	0.026	33 (40)	26 (31)

*Principal *g* values and *g* strains are derived from modeling X- and W-band spectra (see Fig. 2).
†Relative amplitudes are from CW X-band and echo-detected spectra using the DEER detection-pulse sequence. Values from −0.4 V samples are next to those from −0.3 V samples (in brackets). The echo amplitude is dependent upon the electron-spin decay (phase memory) time, so the amplitudes may not equate to the stoichiometries of the reduced clusters.

The term f_A^m describes the extent to which the A (detection) spin is excited by the detection pulse sequence with the field orientation $\mathbf{B}_0^m(\theta,\phi)$, and c_{mod}^m is the corresponding modulation or oscillation depth, describing the extent to which the pump pulse is resonant with the B (pump) spin for $\mathbf{B}_0^m(\theta,\phi)$. To account for the random distribution of molecules in the frozen-solution samples, a summation is performed over all orientations of $\mathbf{B}_0^m(\theta,\phi)$ with respect to the molecular frame.

First, we evaluate qualitatively the experimental DEER traces in Fig. 5. The intercluster distances can be estimated from the dominant periods of oscillation, ranging from 0.5 to 0.7 μs ($\omega_{dd}/2\pi = 2.0$–1.4 MHz). Assuming that the dominant oscillation corresponds to the intense (perpendicular) feature in the powder-averaged dipolar spectrum, and taking reasonable values for the SPFs ($k_{1,2} = 1.35$, $k_{3,4} = -0.85$, see below), then 10 Å equates to 70–150 MHz, 20 Å to 2–5 MHz, 30 Å to 1–3 MHz, and 40 Å to 0.7–1.3 MHz (the exact values depend on the SPF assignments): the traces in Fig. 5 suggest an intercluster distance of ≈20–35 Å. The cluster pairs that contribute most intensity to the observed traces can also be identified. In Fig. 5, traces 3* and 3 (matching traces from samples at −0.3 and −0.4 V, respectively) are essentially identical. Signal N1b is only observed at −0.4 V (see Table 1) so the close match suggests that N1b does not contribute significantly. The DEER electron-spin echo from N5 is not observed at 10 K because it relaxes too rapidly: It contributes only to signal decay, not to the DEER oscillations. The remaining signals, N2, N3, and N4, yield three pairs: N2-N3, N2-N4, and N3-N4. The 4Fe[PS] (N2) and 4Fe[51] (N3) clusters are too far apart (61 Å, see Fig. 1) to contribute more than a weak, indiscernible monotonic decay. In model A the N2-N4 and N3-N4 distances are 49 and 17 Å, in model B 26 and 41 Å, and in model C 14 and 49 Å, respectively. In models A and C neither distance is around 20 to 35 Å, already indicating that model B is most likely.

A quantitative evaluation of each model requires the numerical simulation and analysis of a comprehensive set of DEER traces, as described below. Importantly, because the dipolar frequencies depend on the orientation of a cluster pair with respect to $\mathbf{B}_0$ (as well as on the SPFs and on $1/r^3$), a unique description of the data is only obtained when a sufficient set of orientations are interrogated, by varying the pump and detection pulse positions (see Fig. S1). Fig. 4 depicts the pulse positions used to measure the DEER traces in Fig. 5; additional data, which were included in the analysis, are described in Figs. S2 and S3. Specifically, the simulations (*SI Text* and ref. (19) for details) require the spin Hamiltonian parameters in Table 1, the coordinates and SPFs for each Fe of each paramagnetic cluster, and the *g*-axis orientation for each paramagnetic cluster, relative to the molecular frame. The latter quantities are not known precisely, and our procedures to account for them are described next.

The Fe Coordinates: The Structure of the Hydrophilic Domain from *T. thermophilus* Complex I as a Template for *B. taurus* Complex I. Here, we use the structure of the hydrophilic domain of *T. thermophilus* complex I (2) (the only available structure) as our basis for interpreting EPR data from the *B. taurus* enzyme (the best characterized enzyme spectroscopically). To evaluate our structural model the sequences of the *T. thermophilus* and *B. taurus* core hydrophilic proteins were compared (see *SI Text* for details). The sequence identities and similarities (see Table S1) are high in all cases. The subunits are generally conserved in length, and there are few large alignment gaps (except for in the large domain of the 75 kDa subunit). Multiple sequence alignments and comparative protein models, generated for the *B. taurus* structure, support the close structural identity of the two proteins. They show also that essentially all the insertions/deletions comprise surface loops or structures, and the few that do not are readily

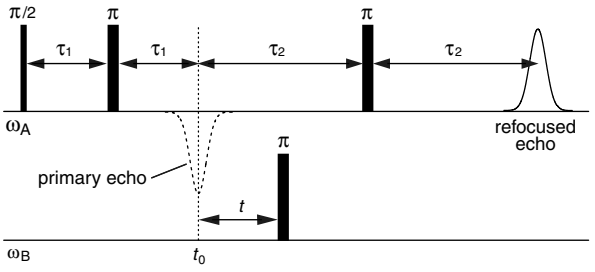

Fig. 3. The four-pulse DEER sequence. The mw detection subsequence at ω_A is applied to the detection (A) spins, and the pump pulse at frequency ω_B is applied to the pump (B) spins. The refocused echo from the detection spins at time $2(\tau_1+\tau_2)$ is observed as a function of time (*t*), where $t_0 = 2\tau_1$ is outside the spectrometer deadtime of ≈100 *ns*.

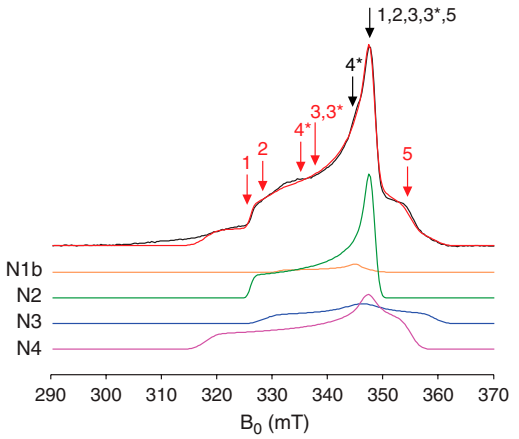

Fig. 4. X-band echo-detected EPR spectrum of complex I reduced to −0.4 V recorded at 10 K and simulated with N1b, N2, N3, and N4. Data in black, simulation (see Table 1) in red. The markers correspond to the pump (*Red*) and detection (*Black*) pulse positions for the DEER traces in Fig. 5. Positions 3* and 4* refer to the −0.3 V sample; all others refer to the −0.4 V sample. See *Experimental Methods* section for the measurement parameters.

Downloaded by guest on October 25, 2021

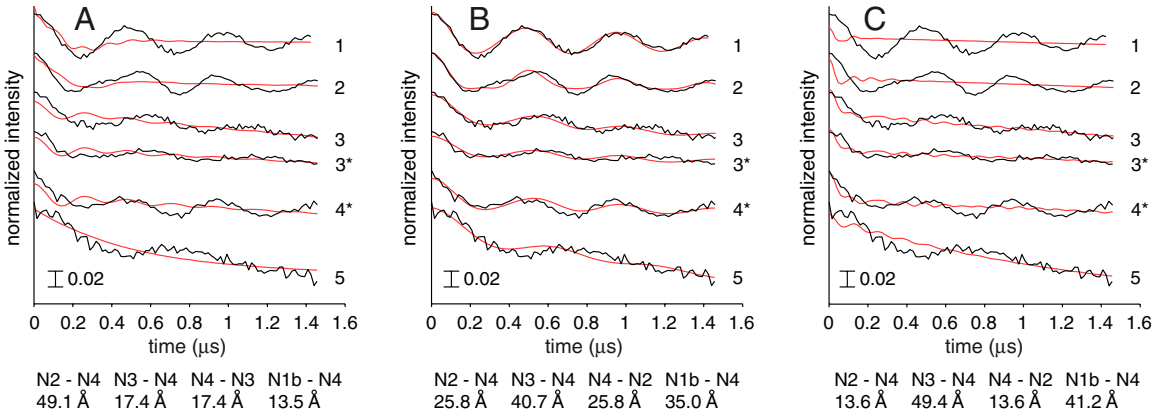

Fig. 5. DEER spectra from *B. taurus* complex I reduced to −0.4 V and −0.3 V measured at 10 K. DEER traces (*Black*) and best-fit simulations (*Red*) for models A, B, and C. Traces 3* and 4* refer to the −0.3 V sample, all others are from the −0.4 V sample, using the following field (mT), detection (ω_A, GHz), and pump (ω_B, GHz) pulse positions (see also Fig. 4): (1) $B_0 = 337.7$, $\omega_A = 9.1104$, $\omega_B = 9.7269$; (2) $B_0 = 340.5$, $\omega_A = 9.1888$, $\omega_B = 9.7267$; (3) $B_0 = 340.4$, $\omega_A = 9.1810$, $\omega_B = 9.4500$; (3*) $B_0 = 345.9$, $\omega_A = 9.3382$, $\omega_B = 9.5998$; (4*) $B_0 = 345.9$, $\omega_A = 9.3382$, $\omega_B = 9.5998$; (5) $B_0 = 347.3$, $\omega_A = 9.3682$, $\omega_B = 9.1888$. All traces are normalized to the intensity at $t = 0$, and intensity changes are denoted by the scale bar. The fits shown are for $k_{1,2} = +1.17$ and $k_{3,4} = -0.67$; the detection-pump spin pairs used in each model are given below the figures, along with the mean intercluster distances.

accommodated without significant alterations in structure (see Fig. S4).

There are three reasons to challenge *T. thermophilus* complex I as a viable structural model for the *B. taurus* enzyme: *i*) the Nqo15 subunit of *T. thermophilus* (2) is not found in *B. taurus*, and the hydrophilic domain of *B. taurus* complex I contains seven subunits that are not found in *T. thermophilus* (7); *ii*) the 75 kDa subunit of *T. thermophilus* complex I ligates a 4Fe cluster (4Fe[75]*) that is not found in *B. taurus*; *iii*) *T. thermophilus* complex I has not been well characterized by EPR, but available spectra (20) do not closely resemble those from *B. taurus* (notably, the g_z component of N4, usually evident at $g \sim 2.10$ (5), has not been observed). Interestingly, the EPR spectra of *E. coli* complex I resemble those from *B. taurus* more closely (21), although the sequence identities between all three species are comparable (see Table S1). *E. coli* complex I does not contain any extra subunits, and it does contain 4Fe[75]*, so neither feature is a significant determinant of the EPR spectrum. Although the immediate cluster environments are very similar in *T. thermophilus* and *B. taurus* complex I, they are not identical (see *SI Text* and Fig. S5) and residue differences close to one or more clusters will affect their spectra and/or reduction potentials (different clusters are reduced in different species). However, it is highly unlikely that these changes affect the structure. Consequently, we consider the cofactor arrangement in *T. thermophilus* complex I an excellent model for the interpretation of spectral data from *B. taurus* complex I.

Spin Projection Factors (SPFs) and *g*-Axis Orientation Combinations. The reduced 2Fe[75] cluster (N1b) has an axial *g* matrix. For completeness we considered two g_3-axis orientations, one along the Fe-Fe vector and one normal to the [2Fe-2S] plane; the g_1 and g_2 axes can take any direction perpendicular to the g_3 axis without changing the simulations (see Fig. 6). In 2Fe clusters like 2Fe[75], it is accepted that strong antiferromagnetic coupling between the Fe^{2+} ($S = 2$) and Fe^{3+} ($S = 5/2$) subsites produces a well separated $S_{total} = 1/2$ ground state, and the SPFs are $k_1(Fe^{2+}) = -4/3$ and $k_2(Fe^{3+}) = +7/3$ (22). However, there are two possible assignments for k_1 and k_2 because the Fe^{2+} and Fe^{3+} could be in either subsite.

In reduced 4Fe clusters there are many possible spin coupling schemes for the (formally) three Fe^{2+} ($S = 2$) and one Fe^{3+} ($S = 5/2$) (23). Mössbauer spectroscopy (24) and theoretical studies (15) have indicated that 4Fe clusters contain delocalized valence electrons distributed over an Fe^{2+}-Fe^{2+} pair ($k_3 = k_4$) and a mixed valence $Fe^{2.5+}$-$Fe^{2.5+}$ pair ($k_1 = k_2$) (see Fig. 6). The six ways of assigning the two pairs produce six arrangements of SPFs, and in each arrangement the g_3-axis is considered perpendicular to both the Fe^{2+}-Fe^{2+} and $Fe^{2.5+}$-$Fe^{2.5+}$ vectors (25, 26). Signal N2 is close to axial, so there are only six possible combinations of *g* axes and SPFs. Signals N3 and N4 have rhombic *g* matrices so the orientations of the g_1 and g_2 axes are important. We tested two generally accepted possibilities: the g_1 and g_2 axes point along the Fe^{2+}-Fe^{2+} and the $Fe^{2.5+}$-$Fe^{2.5+}$ vectors, or they are rotated by 45° (to be normal to the faces that contain an Fe^{2+} and an $Fe^{2.5+}$). Therefore, N3 and N4 both have $6 \times 2 \times 2 = 24$ possible SPF/*g*-axis combinations.

The SPFs of the Fe^{2+} and $Fe^{2.5+}$ pairs in 4Fe clusters are variable also (27). In reduced ferredoxin-type clusters, they may result from the $|5/2|2|1/2\rangle$ state with $k_{1,2} = +1.17$, $k_{3,4} = -0.67$, the $|7/2|3|1/2\rangle$ state with $k_{1,2} = +1.50$, $k_{3,4} = -1.00$, or a mixed state with average values of $k_{1,2} = +1.35$, $k_{3,4} = -0.85$ (notation: spin state of $Fe^{2.5+}$ pair | spin state of Fe^{2+} pair | spin ground state of cluster). All three possibilities were tested. As a sensitivity test we also investigated the $|9/2|4|1/2\rangle$ state ($k_{1,2} = +1.83$, $k_{3,4} = -1.33$) that is thought to contribute to the ground state of aconitase-type clusters. Finally, to ensure a manageable computation time, the SPFs of each 4Fe cluster in a given simulation were the same.

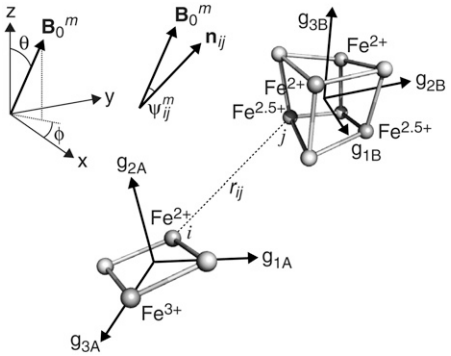

Fig. 6. Orientation selective DEER simulation parameters for a [2Fe-2S]-[4Fe-4S] pair. The unit magnetic field vector, $\mathbf{B}_0^m$, is defined by the angles θ and ϕ. $\mathbf{n}_{ij}$ is the unit vector between Fe ions *i* and *j* of the two clusters, r_{ij} is the distance between them, and ψ_{ij}^m is the angle between $\mathbf{B}_0^m$ and $\mathbf{n}_{ij}$. The g_3 axis from the [2Fe-2S] spin is along the Fe-Fe vector. The g_3 axis from the [4Fe-4S] spin is normal to the faces assigned to the Fe^{2+} and the $Fe^{2.5+}$ pairs, and, in this example, the g_1 and g_2 axes are normal to the Fe^{2+}–$Fe^{2.5+}$ containing faces.

Downloaded by guest on October 25, 2021

In summary, the number of SPF/g-axis orientation combinations are N1b (4), N2 (6), N3 (24), and N4 (24), and there are four sets of 4Fe SPFs. For example, to simulate the N2-N4 pair, there are $6 \times 24 \times 4 = 576$ possible combinations.

Simulation of Observed DEER Traces and Assignment of N4. The observed DEER traces are weighted sums of the refocused echo intensity from each paramagnetic cluster,

$$y_{\mathrm{sim}}^{\mathrm{Tot}}(t) = A^{\mathrm{N2}} y_{\mathrm{sim}}^{\mathrm{N2}}(t) + A^{\mathrm{N3}} y_{\mathrm{sim}}^{\mathrm{N3}}(t) + A^{\mathrm{N4}} y_{\mathrm{sim}}^{\mathrm{N4}}(t) + A^{\mathrm{N1b}} y_{\mathrm{sim}}^{\mathrm{N1b}}(t). \quad [3]$$

The terms A^{Nx} and $y_{\mathrm{sim}}^{\mathrm{Nx}}(t)$ are the refocused echo intensity and the simulated DEER trace (from Eq. **2**) for the detection spin, Nx, respectively. Note that A^{Nx} depends on $\mathbf{B}_0$, but $\mathbf{B}_0$ does not vary during an experiment so A^{Nx} is a constant in Eq. **3**. The N2-N3, N2-N4, and N2-N1b pairs all contribute to $y_{\mathrm{sim}}^{\mathrm{N2}}(t)$, but the N2-N3 and N2-N1b distances (61 and 51 Å, respectively) are too long to yield oscillations (in any model, see Fig. 1), so only N2-N4 is included. The N3–N4 pair is expected to contribute to $y_{\mathrm{sim}}^{\mathrm{N3}}(t)$, but the N3-N2 distance is again too long. The N3-N1b distance is too short (14 Å) and, N1b is present only substoichiometrically, so the oscillation depth, c_{mod}, of the N3-N1b contribution is low. Three pairs, N4-N2, N4-N3 and N4-N1b, may contribute to $y_{\mathrm{sim}}^{\mathrm{N4}}(t)$, but the N4-N1b contribution (like N3-N1b) is only of low intensity. Finally, the contribution from $A^{\mathrm{N1b}} y_{\mathrm{sim}}^{\mathrm{N1b}}(t)$ is small because A^{N1b} is small and only the unknown N1b-N4 distance merits consideration (model A, 13.5 Å; model B, 35.0 Å, and model C, 41.2 Å). Finally, because our simulations do not consider the additional complexity of a single detection spin being influenced simultaneously by two pump spins (the large g-matrix anisotropies make this case unlikely), each simulation comprises only four cluster pairs (one for each detection spin). The pair combinations which were tested are listed in Table S2, and the pairs which produced the best-fit simulations for each model are shown in Fig. 5, along with the intercluster distances.

Finally, each simulated DEER trace from Eq. **3** is dampened by an exponential decay to account for signal relaxation, and a baseline offset is added, to account for unmodulated intensity that is not correctly described (resulting primarily from inaccuracies in A^{Nx} and the g-axis orientations). The residual, R, is calculated by Eq. **4**, and the best fits to the data traces, $y_{\mathrm{exp}}(t)$, were identified by inspecting the fits with the lowest squared residual values (the sum of R^2 over all the DEER traces):

$$R = y_{\mathrm{exp}}(t) - (c_1 y_{\mathrm{sim}}^{\mathrm{Tot}}(t) \exp(-t/T) + c_2) \quad [4]$$

The DEER simulation algorithm has been described previously (19), and its particular application to a set of FeS clusters is summarized in *SI Text*. In accord with previous work on, for example, NO radicals (12), we chose to fit our data directly in the time domain, to allow simultaneous fitting of both the baseline and the DEER oscillation, and to avoid difficulties associated with the Fourier transformation of DEER traces with large unmodulated contributions. First, an initial screen was used to test all possible combinations of the SPFs, g-axis orientations and cluster pairs, for each model. The constant c_2 was included to maximize the sensitivity to the oscillation period (to the SPFs and the intercluster distances). The initial screen excluded ≈95% of the combinations. Then, the remaining combinations were reduced by examining fits with $c_2 = 0$, to maximize the sensitivity to the oscillation depth (to the g-axis orientations). The best fits to the data, for each of models A, B, and C (see Fig. 1), are displayed in Fig. 5*A*, *B*, and *C*, respectively.

The fits shown in Fig. 5 (additional data are shown in Fig. S3) include c_2, so they are most sensitive to the oscillation period. Clearly, model B describes the experimental data well, but models A and C produce only simulations with completely inappropriate oscillation periods: the intercluster distances in models A and C are entirely inconsistent with the data. In contrast, ≈1% of the total number of possible combinations produced satisfactory fits for model B. All these fits contained the same g-axis orientations for N4 and N2 (see Fig. S6). Changing the g-axis orientation of N3 had little effect because the N3–N4 distance is too long; changing the SPFs for N1b had essentially no effect. The best-quality fits (see Fig. 5*B*) used the SPFs from the $|5/2|2|1/2\rangle$ state, but those from the mixed $|7/2|3|1/2\rangle$ and $|5/2|2|1/2\rangle$ state produced similar quality fits. The $|7/2|3|1/2\rangle$ state produced only lower quality fits, and the $|9/2|4|1/2\rangle$ state did not produce any satisfactory fits. Imperfections in the best fits from model B may arise from small inaccuracies in the structural model (for example, a cluster may be tilted slightly in the *B. taurus* enzyme, relative to in *T. thermophilus*), or from our imprecise knowledge of the g-axis orientations and SPFs (see Fig. S7). These uncertainties limit the accuracy of our data fits, but they do not detract from the unambiguous assignment of signal N4 to the 4Fe[TY]1 cluster (position 5). DEER clearly discriminates between the models because of its $1/r^3$ sensitivity to distance.

We conclude that N4 originates from the reduced 4Fe[TY]1 cluster in complex I (position 5) and thus model B is correct.

Discussion

The application of DEER to measure the distances between complex paramagnetic metal centers in enzymes is a natural extension from established studies of the distances between organic $S = 1/2$ radicals (11–13). In reduced complex I there are five paramagnetic FeS clusters, and it would be unrealistic to attempt to define their spatial relationships *ab initio* using DEER. Not only do five interacting paramagnets lead to a complicated network of relationships, but the complex magnetic interactions within the clusters and the orientation selectivity of individual DEER measurements complicate the analysis significantly—for even a single pair of clusters. Here, we combine DEER spectroscopy with a structural model for the FeS cluster ensemble. Our success has relied on using structural information to restrict both the spatial arrangements of the paramagnetic centers and the g-axis orientations. Our results present a definitive assignment of EPR signal N4 to a structurally defined cluster in complex I, because they are based on direct measurements, rather than on data from overexpressed subunits and subcomplexes—which may not retain their structural or spectral integrity.

Our analysis concludes unambiguously that N4 derives from 4Fe[TY]1 (position 5), as suggested by Hirst and coworkers (5), and supports the consensus assignment of N1b to 2Fe[75] (position 2), N2 to 4Fe[PS] (position 7), and N3 to 4Fe[51] (position 1). It is entirely inconsistent with the assignment of N4 to 4Fe[75]C (position 3), as contended by Ohnishi et al. (3, 4), or with the assignment of N4 to 4Fe[TY]2 (position 6), an alternative suggestion by Hirst and coworkers (5). Although our analysis does not address directly the assignment of N5, mutation of the histidine ligand of 4Fe[75]H to alanine did not affect N5 in *Yarrowia lipolytica* complex I (although it did prevent catalysis) (28). Therefore, the assignment of N5 to 4Fe[75]H (position 4) by Ohnishi et al. (3, 4) is not correct. Hirst and coworkers concurred that N5 derives from the 75 kDa subunit but assigned it instead to 4Fe[75]C (position 3) (5), an assignment that is consistent with all extant data and with the analysis described here. Signal N5 is unusual: it is observed only in a subset of eukaryotic enzymes, and it relaxes more rapidly at −0.4 V than at lower potential (6).

The assignment of EPR signals to structurally defined clusters (model B, see Fig. 1) provides an alternating or 'roller-coaster' potential energy profile for electron transfer along the cluster chain between the active sites. Alternating the low and high potential clusters optimizes the rate at which a single electron traverses the empty chain, whereas two or more adjacent low potential clusters would impede electron transfer significantly (8). Furthermore, in the mitochondrial matrix the NAD^+ pool is typically 90% oxidized, and, because NADH/NAD^+

Downloaded by guest on October 25, 2021

interconversion and intramolecular electron transfer in complex I are fast, the FeS clusters are probably, on average, reduced to the NAD^+ potential (≈ -0.3 V) during turnover. Consequently, four electrons occupy the seven FeS cluster chain [for N3 (4Fe[51]), N5 (4Fe[75]C), and N4 (4Fe[TY]1) $E_{pH7} = -0.25$ V; for N2 (4Fe[PS]) $E_{pH7} = -0.1$ V (3)]; the other three clusters are oxidized. An alternating occupancy along the chain (positions 1, 3, 5, and 7) further optimizes the rate at which an electron is transferred out to quinone, following input of an electron from the flavin (in analogy to the Grotthuss mechanism for proton transfer). More importantly, the alternating occupancy may be key to efficient energy conversion by complex I; the energy of the incoming electron is conserved in the outgoing electron (in analogy to the conservation of energy in Newton's cradle), allowing close to the full redox potential drop from NADH to quinone to be trapped in proton translocation.

Experimental Methods

Preparation of EPR Samples of Complex I from *B. taurus*. Complex I was isolated from *B. taurus* heart tissue as described previously (29), except ethylene glycol, not glycerol, was used in the membrane preparation, phenylmethanesulfonyl fluoride was omitted, and asolectin was omitted from the ion-exchange chromatography. Where possible ultrapure chemicals (Fluka) were used, to minimize contamination by manganese and eliminate the Mn^{2+} signal from W-band spectra. The ultrapure chemicals were dithiothreitol (Mn $\leq$ 5 ppm), ethylenediaminetetraacetic acid (Mn $\leq$ 5 ppm), ethylene glycol (Mn $\leq$ 0.05 ppm), KCl (Mn $\leq$ 0.01 ppm), NaCl (Mn $\leq$ 0.01 ppm), and Trizma base (Mn $\leq$ 5 ppm). Purified complex I was concentrated to ~70 mg mL^{-1} (quantified by the Pierce bicinchoninic acid assay) using Vivaspin centrifugal concentrators with a 100 kDa cutoff, and imported into an anaerobic glovebox ($O_2 \sim 2$ ppm). Typically, it was reduced by 10 mM NADH (to ≈ -0.4 V), or by 140 mM NAD^+ and 2 mM NADH (to ≈ -0.3 V), to a final concentration of ~55 mg mL^{-1} (~55 μM), then the samples were frozen anaerobically in liquid nitrogen.

EPR Spectroscopy. X-band CW EPR experiments were performed on a Bruker BioSpin GmbH EMX spectrometer equipped with a high sensitivity Bruker probehead and a low-temperature Oxford Instruments CF935 helium-flow cryostat. The magnetic field was calibrated at room temperature with an external 2,2-diphenyl-1-picrylhydrazyl standard ($g = 2.0036$). Experiments were conducted at 12 K, with 0.5 mW power, and 0.5 mT amplitude at 100 kHz. Pulsed EPR measurements were performed on a W-/X-band Bruker Elexsys 680 spectrometer using a Bruker 3 mm split ring resonator (ER-4118X_MS3) at X-band and a EN600-1021H TeraFlex resonator at W-band, both equipped with an Oxford Instruments cryostat and a variable temperature unit. DEER measurements employed a four pulse sequence, $\boldsymbol{\pi}/2$–τ_1–$\boldsymbol{\pi}$–τ_1–τ_2–$\boldsymbol{\pi}$–τ_2–echo, for the detection pulses at frequency ω_A, and a single pump pulse at frequency ω_B moved within the refocused echo sequence (see Fig. 3). The detection pulses were phase cycled according to $[+x, +y, +y, +, -x, +y, +y, -]$, and employed lengths of $t_{\boldsymbol{\pi}}/t_{\boldsymbol{\pi}/2} = 40$ ns/40 ns. The pump pulse ($t_{\boldsymbol{\pi}}$) had a duration of either 16, 20, or 24 ns, depending on the achievable excitation magnetic (B_1) field. A variable τ_1 time (from 140–164 ns, or from 180–204 ns) was applied to dampen nuclear modulations, and time τ_2 was 1.1–1.6 μs. Echo-detected EPR spectra were recorded by integrating the echo intensity either from a refocused echo (using the same parameters as in the DEER experiments), or from the pulse sequence $\boldsymbol{\pi}/2$–τ–$\boldsymbol{\pi}$–τ–echo, with $t_{\boldsymbol{\pi}/2} = 48$ ns, $t_{\boldsymbol{\pi}} = 96$ ns, and $\tau = 200$ ns at X-band, and with $t_{\boldsymbol{\pi}/2} = 24$ ns, $t_{\boldsymbol{\pi}} = 48$ ns, and $\tau = 140$ ns at W-band. All pulsed X-band experiments were carried out at 10 K with a repetition time of 2 ms, and W-band measurements were performed at 8.5 K with a repetition time of 1.5 ms.

ACKNOWLEDGMENTS. This work was supported by the Medical Research Council and the Engineering and Physical Sciences Research Council (Grant EP/D044855D/1 supporting the Oxford Center for Advanced Electron Spin Resonance).

1. DiMauro S, Schon EA (2003) Mitochondrial respiratory-chain diseases. *New Engl J Med*, 348:2656–2668.
2. Sazanov LA, Hinchliffe P (2006) Structure of the hydrophilic domain of respiratory complex I from *Thermus thermophilus*. *Science*, 311:1430–1436.
3. Ohnishi T (1998) Iron-sulfur clusters/semiquinones in complex I. *Biochim Biophys Acta*, 1364:186–206.
4. Ohnishi T, Nakamaru-Ogiso E (2008) Were there any "misassignments" among iron-sulfur clusters N4, N5 and N6b in NADH-quinone oxidoreductase (complex I)?. *Biochim Biophys Acta*, 1777:703–710.
5. Yakovlev G, Reda T, Hirst J (2007) Reevaluating the relationship between EPR spectra and enzyme structure for the iron-sulfur clusters in NADH-quinone oxidoreductase. *Proc Natl Acad Sci USA*, 104:12720–12725.
6. Reda T, Barker CD, Hirst J (2008) Reduction of the iron-sulfur clusters in mitochondrial NADH:ubiquinone oxidoreductase (complex I) by Eu^{II}-DTPA, a very low potential reductant. *Biochemistry*, 47:8885–8893.
7. Hirst J, Carroll J, Fearnley IM, Shannon RJ, Walker JE (2003) The nuclear encoded subunits of complex I from bovine heart mitochondria. *Biochim Biophys Acta*, 1604:135–150.
8. Page CC, Moser CC, Chen X, Dutton PL (1999) Natural engineering principles of electron tunnelling in biological oxidation-reduction. *Nature*, 402:47–52.
9. Sled VD, Rudnitzky NI, Hatefi Y, Ohnishi T (1994) Thermodynamic analysis of flavin in mitochondrial NADH:ubiquinone oxidoreductase (complex I). *Biochemistry*, 33:10069–10075.
10. Yano T, Dunham WR, Ohnishi T (2005) Characterization of the $\Delta\mu H^+$-sensitive ubisemiquinione species (SQ_{NF}) and the interaction with cluster N2: New insight into the energy-coupled electron transfer in complex I. *Biochemistry*, 44:1744–1754.
11. Jeschke G (2002) Distance measurements in the nanometer range by pulse EPR. *Chemphyschem*, 3:927–932.
12. Jeschke G, Koch A, Jonas U, Godt A (2002) Direct conversion of EPR dipolar time evolution data to distance distributions. *J Magn Reson*, 155:72–82.
13. Chiang Y-W, Borbat PP, Freed JH (2005) Maximum entropy: A complement to Tikhonov regularization for determination of pair distance distributions by pulsed ESR. *J Magn Reson*, 177:184–196.
14. Bertrand P, et al. (1994) Biological polynuclear clusters coupled by magnetic interactions—from the point dipole approximation to a local spin model. *J Am Chem Soc*, 116:3078–3086.
15. Noodleman L, Peng CY, Case DA, Mouesca JM (1995) Orbital interactions, electron delocalization and spin coupling in iron-sulfur clusters. *Coord Chem Rev*, 144:199–244.
16. Elsässer C, Brecht M, Bittl R (2002) Pulsed electron-electron double resonance on multinuclear metal clusters: Assignment of spin projection factors based on the dipolar interaction. *J Am Chem Soc*, 124:12606–12611.
17. Elsaesser C, Brecht M, Bittl R (2005) Treatment of spin-coupled metal-centers in pulsed electron-electron double-resonance experiments. *Biochem Soc Trans*, 33:15–19.
18. Stoll S, Schweiger A (2006) EasySpin, a comprehensive software package for spectral simulation and analysis in EPR. *J Magn Reson*, 178:42–55.
19. Lovett JE, et al. (2009) Structural information from orientationally selective DEER spectroscopy. *Phys Chem Chem Phys*, 11:6840–6848.
20. Hinchliffe P, Carroll J, Sazanov LA (2006) Identification of a novel subunit of respiratory complex I from *Thermus thermophilus*. *Biochemistry*, 45:4413–4420.
21. Leif H, Sled VD, Ohnishi T, Weiss H, Friedrich T (1995) Isolation and characterization of the proton-translocating NADH:ubiquinone oxidoreductase from *Escherichia coli*. *Eur J Biochem*, 230:538–548.
22. Gibson JF, Hall DO, Thornley JHM, Whatley FR (1966) The iron complex in spinach ferredoxin. *Proc Natl Acad Sci USA*, 56:987–990.
23. Beinert H, Holm RH, Münck E (1997) Iron-sulfur clusters: Nature's modular, multipurpose structures. *Science*, 277:653–659.
24. Münck E, Popescu CV (2000) Mössbauer studies of exchange coupled cluster assemblies in biological systems. *Hyperfine Interact*, 126:59–67.
25. Kamlowski A, van der Est A, Fromme P, Stehlik D (1997) Low temperature EPR on Photosystem I single crystals: Orientation of the iron-sulfur centers FA and FB. *Biochim Biophys Acta*, 1319:185–198.
26. Gloux J, Gloux P, Lamotte B, Mouesca J-M, Rius G (1994) The different $[Fe_4S_4]^{3+}$ and $[Fe_4S_4]^{+}$ species created by γ-irradiation in single crystals of the $(Et_4N)_2[Fe_4S_4(SBenz)_4]$ model compound: Their EPR description and their biological significance. *J Am Chem Soc*, 116:1953–1961.
27. Mouesca JM, Noodleman L, Case DA, Lamotte B (1995) Spin-densities and spin coupling in iron-sulfur clusters—a new analysis of hyperfine coupling-constants. *Inorg Chem*, 34:4347–4359.
28. Waletko A, et al. (2005) Histidine 129 in the 75 kDa subunit of mitochondrial complex I from *Yarrowia lipolytica* is not a ligand for $[Fe_4S_4]$ cluster N5 but is required for catalytic activity. *J Biol Chem*, 280:5622–5625.
29. Sharpley MS, Shannon RJ, Draghi F, Hirst J (2006) Phospholipid interactions determine the catalytic activity of NADH:ubiquinone oxidoreductase (complex I) from bovine mitochondria. *Biochemistry*, 45:241–248.

Downloaded by guest on October 25, 2021